

Rethinking Radiology Report Generation via Causal Reasoning and Counterfactual Augmentation

Xiao Song¹, Jiafan Liu², Yun Li³, Wenbin Lei³, Ruxin Wang^{†,1}

¹Shenzhen Institute of Advanced Technology, Chinese Academy of Sciences

²South China Agricultural University

³The First Affiliated Hospital, Sun Yat-sen University

{x.song.matt;jiagonglou21}@gmail.com; {liyun76; leiwb}@mail.sysu.edu.cn; rx.wang@siat.ac.cn

Abstract

Radiology Report Generation (RRG) draws attention as an interaction between vision and language fields. Previous works inherited the ideology of vision-to-language generation tasks, aiming to generate paragraphs with high consistency as reports. However, one unique characteristic of RRG, the independence between diseases, was neglected, leading to the injection of the spurious confounder, i.e., the disease co-occurrence. Unfortunately, this confounder confuses the process of report generation worse because of the biased RRG data distribution. In this paper, to rethink this issue thoroughly, we reason about its causes and effects from a novel perspective of statistics and causality, where the Joint Vision Coupling and the Conditional Sentence Coherence Coupling are two aspects prone to implicitly decrease the accuracy of reports. Then, a counterfactual augmentation strategy that contains the Counterfactual Sample Synthesis and the Counterfactual Report Reconstruction sub-methods is proposed to break these two aspects of spurious effects. Experimental results and further analyses on two widely used datasets justify our reasoning and proposed methods.

1. Introduction

With the aim of helping radiologists decrease their workloads caused by the explosive demand growth of radiological examination, Radiology Report Generation (RRG) has attracted obviously increasing attention recently in the fields of medicine and its combination with vision and language. RRG could be considered as a specific type of cross-modal translation [1], which firstly recognizes the visual features of the radiograph and then produces a long paragraph as a report based on the recognition results. The report of RRG

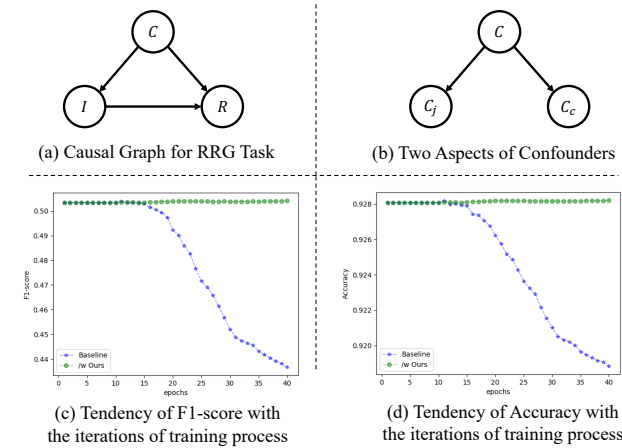


Figure 1. (a) is the causal graph for the RRG model where the co-occurrence is a confounder in the process of report generation. (b) indicates that the co-occurrence could be divided into two aspects, i.e., the Joint Vision Confounder C_j and the Conditional Sentence Coherence Confounder C_c . (c) and (d) respectively present the smoothed tendencies of F1-score and Accuracy of the generated reports with the progresses of training epochs on IU X-Ray datasets.

contains a series of sentences of which each one describing certain types of independent normal or abnormal anatomic structures [10, 28].

Recent methods [14, 18, 31, 35, 36] followed the ideology of traditional machine translation and image-to-text generation tasks like Image Captioning [12, 30], aiming to generate a paragraph with high consistency. Specifically, Li et al. [14] proposed a knowledge-driven encode, retrieve, and paraphrase approach that learns to enhance the relations between anatomic terminologies with Graph Transformer. Zhang et al. [36] assumed that abnormalities on the same body part might have a strong correlation with each other and share many features, thus they proposed a

[†]Corresponding Author.

Codes will be public available after acceptance.

knowledge graph that groups chest diseases occurring in the same organ or tissue for assisting radiology report generation. Liu et al. [18] proposed a prior knowledge explorer to find the most relevant chest terminologies from that knowledge graph [36] and to match the language from the existing report corpus, which improves the report consistency. Wang et al. [31] enforced the co-occurrence of chest terminologies to be incorporated into the final reports. These methods improved RRG model performance, particularly in metrics of Natural Language Generation (NLG) that evaluate the paragraph consistency, which boosted the co-occurrence injection to be a common strategy in RRG.

Despite recent progress, there remains a fundamental unique characteristic of RRG neglected, i.e., the independence between diseases, which makes disease co-occurrence a confounder conforming to the Simpson’s paradox [23] in the RRG task as shown in Fig. 1 (a). This characteristic could be divided into two aspects of coupling confounders, i.e., the Joint Visual Coupling C_j and the Conditional Sentence Coherence Coupling C_c as shown in Fig. 1 (b). Specifically, on the one hand, this spurious co-occurrence will result in the one-to-many coupling C_j of radiograph visual features to the recognition of diseases. On the other hand, as aforementioned, each sentence in the RRG report independently describes the certain types of diseases [28] and there should be no sequence order between sentences in the free-text reports. However, the spurious sentence coherence coupling C_c was injected previously for improving the consistency, which leads to the spurious co-occurrence of diseases in certain attributes. Either of these spurious couplings injected into the RRG models improved the linguistic consistency and created a semblance boomerang of RRG performance, but the accuracy, a more critical metric for both patients and radiologists, was damaged as shown in the Fig. 1 (c) and (d) where the F1-score and Accuracy of generated reports decline with the iterations of training process.

To rethink these problems thoroughly, we reason about the causes and effects of the disease co-occurrence relationship from a novel perspective of statistics and causality. Specifically, we first find the cause of disease co-occurrences and discuss whether it is beneficial to RRG in a novel perspective of statistics with Simpson’s paradox. Then, the two aspects of effects shown in Fig. 1 (b) are explored with causal graphs, where the Joint Vision Coupling C_j and the Conditional Sentence Coherence Coupling C_c are implicitly decreasing the accuracy of reports. Based on the rethinking and reasoning of co-occurrences in RRG, we propose an easy-but-effective general counterfactual augmentation strategy to solve the problems model-free, which contains two sub-methods specifically. From the aspect of C_j , a Counterfactual Sample Synthesis (CSS) method which randomly masks visual features and their

corresponding sentences in the recognition process is proposed to address the one-to-many visual features coupling and improve the independence between visual feature and disease label pairs. Simultaneously, from the aspect of C_c , we propose a Counterfactual Report Reconstruction (CRR) method that effectively addresses the conditional coupling between sentences. Experimental results and further analyses on two widely used datasets, IU X-Ray [7] and MIMIC-CXR [11], demonstrate the capability of both sub-methods to improve the accuracy of generated reports and achieve better performance when combined together.

Overall, our contributions are as follows:

- To our knowledge, we are the first to discuss the independence of diseases in the RRG task and explore the effects of the two spurious confounders, i.e., the Joint Vision Coupling C_j and Conditional Sentence Coherence Coupling C_c , on RRG models from a novel perspective of statistic and causality. We also propose a novel temporal causal graph to model the causal effect of C_c during the process of report generation.
- We propose an easy-but-effective general counterfactual augmentation method that contains the Counterfactual Sample Synthesis and the Counterfactual Report Reconstruction sub-methods to solve the two problems caused by the two spurious coupling confounders respectively.
- Experiments conducted on two widely used datasets and further result analyses demonstrate the value of our rethinking on RRG task and the ability of our proposed methods to solve these problems.

2. Rethinking

Disease co-occurrence has been widely used in previous works, which improved the performance of Radiology Report Generation (RRG) models, especially on the Natural Language Generation (NLG) metrics. However, such relation was extracted by grouping the diseases happened in the same organs [36], thus it is of significance to clarify whether it is truly beneficial to the qualities of report generation. Additionally, while NLG metrics adopted previously as the main indicators of RRG task are important, it is worth noting that we believe the accuracy of the generated reports is more critical for both radiologists and patients.

To explore the causes and effects of disease co-occurrence, we conduct the rethinking and reasoning to answer the following research questions that are of importance to RRG task.

- Why is the disease co-occurrence a spurious confounder in RRG?
- What effects will the disease co-occurrence exactly have on RRG?

Table 1. Data distribution bias of *Pleural Effusion* (B) conditioned on *Pneumothorax* (A), i.e., $P(B^*|A^*)$, in MIMIC-CXR datasets when grouping diseases based on either normal or abnormal, which is an example that conforms to Simpson’s paradox. * contains '+' and '−', denoting abnormal and normal respectively.

	A^+	A^-	A
	7667	195425	203092
B^+	3552(0.463)	30988(0.159)	-
B^-	1345(0.175)	153822(0.787)	-
B	-	-	189707(0.934)

2.1. Simpson’s Paradox of Co-occurrence

Simpson’s paradox is a statistical phenomenon where an association that holds for an entire population is revised when the population is divided into sub-populations, such as a well-known example of Simpson’s paradox which is a study of gender bias in UC Berkeley’s graduate admissions [3]. Neglecting Simpson’s paradox in data distribution poses a serious risk of wrong strategies to decision-makers since it might lead to misunderstanding spurious relations for causality [32].

In RRG, co-occurrence is one of the variables widely utilized to improve the NLG abilities, yet it conforms to Simpson’s paradox as illustrated in Tab. 1. Based on the assumption that accuracy is more critical if models are employed in medical scenes, we specifically select two types of diseases, i.e., the *Pneumothorax* (A) and the *Pleural Effusion* (B) [18, 36], and explore the conditional probabilities of B given A, denoted as $P(B^*|A^*)$, when grouping them into sub-populations based on either the diseases are normal or abnormal. From Tab. 1, we can find that the disease co-occurrence is a confounder because A and B are co-occurring in the entire population and the both-normal sub-population, but are revising in other sub-populations.

Due to the conforming to Simpson’s paradox, RRG models tend to describe the diseases with higher paragraph consistency. However, the accuracy might simultaneously be declined because models can adapt to this spurious relation more easily rather than excavate the causalities. Thus, the disease co-occurrence conforming to Simpson’s paradox could be the answer to the first question about why it is a spurious confounder in RRG.

2.2. Causal Graphs and Causal Effects

To further explore what effects the disease co-occurrence has on the RRG task, we conduct further analyses with causal graphs from two aspects, i.e., the Joint Vision Coupling C_j and the Conditional Sentence Coherence Coupling C_c . Causal graph is an efficient way of describing the causal relationships between variables, which is represented as directed acyclic graphs $G = \{V, E\}$ with the set of variables

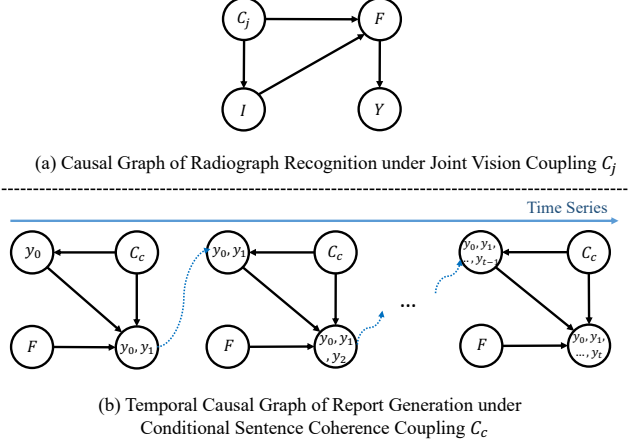


Figure 2. (a) and (b) are causal graphs under the Joint Vision Coupling C_j and the Conditional Sentence Coherence Coupling C_c . C_j and C_c respectively effects the radiograph recognition and report generation processes through backdoor paths.

V and the causal-effect relationships E . Fig. 1 (a) shows the example of causal graph of RRG task which contains three variables X , C and Y . $X \rightarrow Y$ is a causal path indicating the direct effect of X to Y . $X \leftarrow C \rightarrow Y$ is a backdoor path that introduces indirect spurious correlation from X to Y , where C is a confounder. Based on Fig. 1 (b) and the previous analyses, we model the causal relationships under C_j and C_c with the causal graph in Fig. 2.

2.2.1 Effects of Joint Vision Coupling

Like Image Captioning [1], RRG could be considered as a cross-modal translation task that firstly recognizes the contents of radiographs and then generates reports based on the recognition results. Instead of directly effecting the outputs Y , C_j implicitly effects the recognition process. Fig. 2 (a) shows the causal effects in the recognition process, where X is the input radiographs, Y is the generated reports, C_j is the spurious co-occurrence relationship, and F is the recognition results. However, except the visual information from X , F is simultaneously indirectly effected by the spurious co-occurrence relationship C_j through the indirect backdoor path $I \leftarrow C_j \rightarrow F$.

Additionally, based on the fact that radiology reports contain descriptions for both normal and abnormal anatomic structures, recent works [15, 17, 27] pointed out that the normal descriptions are the mainstream in datasets while abnormal ones are the minority, and our statistical comparisons in Tab. 1 demonstrate this assumption, where the normal data dominates the whole distribution. These biased data distributions will exacerbate the impact of C_j .

To sum up, the joint coupling of visual features C_j is a spurious confounder in RRG task and it even gets more

toxic because of the domination of the mainstream normal sub-population, leading to the one-to-many effect of visual features on the disease recognition and the breaking of independence between visual features and disease pairs, which could be denoted as $P(AB) \neq P(A)P(B)$. For example, some spurious co-occurrence relations of two certain types of diseases, such as *Pneumothorax* and *Pleural Effusion*, in entire datasets are caused by the mainstream normal sub-population while minority abnormal sub-population holds weak force to break this spurious relations.

2.2.2 Effects of Conditional Sentence Coherence Coupling

Relatively, C_c effects the process of translation from the recognition results into linguistic reports. Following the idea in [37], we propose a novel temporal causal graph for the report generation process, with each timestep generating one token y_t conditioned on the recognition results F and the previously generated tokens $\{y_0, y_1, \dots, y_{t-1}\}$. However, as shown in Fig. 2 (b), C_c takes the role of a confounder in each timestep, having a spurious sentence coherence effect on the generation process through the backdoor path $\{y_0, y_1, \dots, y_{t-1}\} \leftarrow C_c \rightarrow \{y_0, y_1, \dots, y_t\}$. This spurious effect breaks the independence between sentences, which could be denoted as $P(B|A) \neq P(A)$.

Unfortunately, this spurious sentence coherence was widely accepted as an important quality in the RRG task for guaranteeing the readability of the generated reports [10, 28]. To improve that, Chen et al. [6] proposed a relational memory module that memorized similar patterns in reports and used them as references to help the generation process. Song et al. [27] and Liu et al. [18] proposed to match the report corpus with visual similarities. However, as aforementioned in Sec. 1, RRG models generate multi-sentence reports with each sentence independently describing certain types of diseases [10, 28]. By storing and utilizing those ready-made report corpus in datasets, while the sentence coherence of the generated reports was boosted, some meaningless and spurious inter-sentence coherence was thereto introduced into models, such as the confusing interactions of two sentences.

Theoretically, most RRG models supervised by the ground-truth reports have essentially broken the independence between sentences or rather diseases, where the sequence order is optimized except for token correctness. Thus, harmful inter-sentence coherence is introduced and strengthened during training. This leads to conditional coupling of sentences and diseases, especially with biased data dominated by the mainstream sub-population. This implicit injection of sentence coherence might lead to the declining f1 and accuracy scores on generated reports during training iterations shown in Fig. 1 (c) and (d). Specifically, if the rel-

ative order of two sentences is highly frequent in the data, models may learn to generate the next sentence solely based on the previous one, ignoring the visual input.

3. Methodology

3.1. Modeling Radiology Report Generation

Given a radiograph I , the goal is to generate a long medical report $\tilde{Y} = \{\tilde{y}_1, \tilde{y}_2, \dots, \tilde{y}_T\}$ with T word tokens that describes the information of diseases shown in the radiograph. Thus, the Radiology Report Generation (RRG) task aims to learn the parameters θ of model by maximizing the probability of the correct description:

$$\theta^* = \arg \max \sum \log p(Y|I; \theta). \quad (1)$$

where $Y = \{y_1, y_2, \dots, y_T\}$ is the ground-truth report. Thus, it is common to apply the chain rule to model the joint probability over $\{y_1, y_2, \dots, y_T\}$:

$$\log p(Y|I) = \sum \log p(y_t|I, y_{1:t-1}). \quad (2)$$

Algorithm 1: CoA Algorithm for RRG

Input: original Training Data $D_o = (I, Y)$.
Output: counterfactual training data $D = D_o \cup D_c$ from
CSS and **CRR**.

```

1 Function Main( $D_o$ ) :
2   Function CSS( $I, Y$ ) :
3     a binary feartrue extraction model BFE
4     pretrained on ImageNet and  $D_o$ 
5     a report labeler model LE
6      $F \leftarrow \mathbf{BFE}(I)$ 
7      $s, Y^- \leftarrow$  random pop one sentence in  $Y$ 
8      $l \leftarrow \mathbf{LE}(s)$ 
9      $F^- \leftarrow$  mask  $f$  in  $F$  with label as  $l$ 
10    return ( $F^-, Y^-$ )
11  Function CRR( $Y^-$ ) :
12     $Y^+ \leftarrow$  random disruption  $Y^-$ 
13    return ( $Y^+$ )
14  for  $i$  in  $1, 2, \dots, N$  do
15     $(I, Y) \leftarrow i$ -th data in  $D_o$ 
16     $F^-, Y^- \leftarrow \mathbf{CSS}(I, Y)$ 
17     $Y^+ \leftarrow \mathbf{CRR}(Y^-)$ 
18     $D_c \leftarrow (F^-, Y^+)$ 
19  end
20   $D = D_o \cup D_c$ 
21  return  $D$ 

```

3.2. Counterfactual Augmentation

Counterfactual augmentation (CoA) which produces augmented data by making counterfactual modifications to

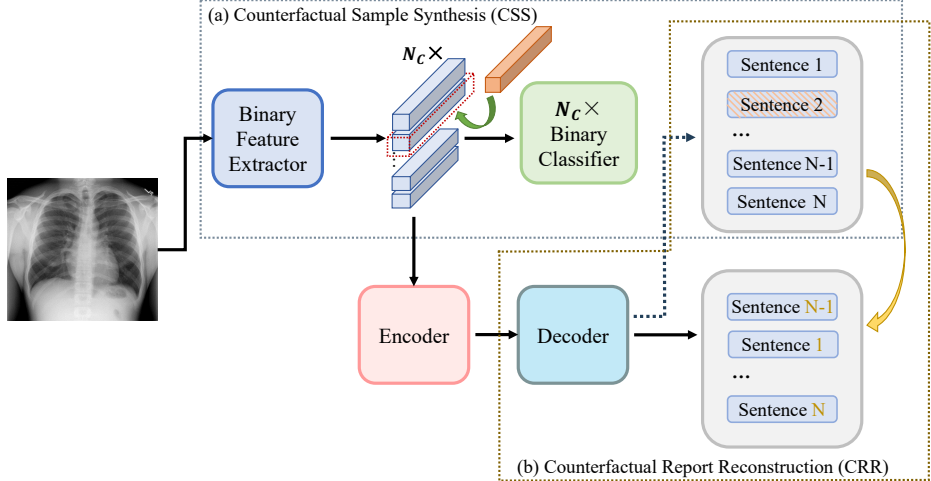


Figure 3. Overview of our proposed CoA method, which totally contain two sub-method, i.e., the CSS and the CRR. Specifically, CSS randomly mask several types of binary features and their corresponding describing sentences and CRR randomly breaking the order of sentences in the reports. These two sub-methods can be integrated together.

a subset of causal factors [24] has recently emerged as a method to mitigate confounding biases in the training data for a machine learning model [20]. In this paper, we focus on analysing the spurious disease co-occurrences in RRG task and manage to solve the problems using model-free general CoA methods. As shown in Alg. 1 and the overall framework in Fig. 3, we first propose a Counterfactual Sample Synthesis (CSS) strategy to decouple the joint vision confounder, and then propose a Counterfactual Report Reconstruction (CRR) strategy to break the conditional sentence coherence confounder.

3.2.1 CSS

The coupling of visual information is a spurious confounder that causes the joint effects of diseases. To break the spurious visual confounder in Radiology Report Generation (RRG) data, we propose a Counterfactual Sample Synthesis strategy which contains two modules, i.e., the Binary Feature Extraction (BFE) module and the Counterfactual Sample Synthesis (CSS) module.

Binary Feature Extraction. Counterfactual sample synthesis methods have been applied in the field of natural image processing tasks [4]. However, contrast to the natural images which is much easier and more mature to be exactly processed with the methods like Object Detection or Semantic Segmentation, radiographs containing dozens of diseases are hard to be accurately detected or segmented. Besides, the anatomic structures of some certain types of diseases are frequently overlapping together, so it is noisy and unrealizable to identify each disease independently. Thus, the counterfactual augmentation methods that made great achievements in natural image processing can not be ap-

plied in the RRG task.

To solve these problems, in this paper, instead of directly processing in the image level, we novelly propose to conduct the counterfactual sample synthesis in the binary feature level, where each binary feature represents one independent type of disease. In this way, we can precisely process every type of disease feature while keeping other features maintaining.

As illustrated in Fig. 3 and Alg. 1, given a training, we first train a Binary Feature Extraction (BFE) model on the original datasets with N_c category binary classification:

$$\{cls_i\}_{i=1}^{N_c} \propto \exp(BC_i(BFE_i(I))), \quad (3)$$

where $BC(\cdot)_i$ is the i -th binary classifier that produces the binary classification result based on the binary features extracted by $BFE(\cdot)_i$. Then, we extract the binary features of radiographs I using the pretrained BFE model as follows:

$$F = \{f_i\}_{i=1}^{N_c} \leftarrow BFE_i(I), \quad (4)$$

Thus, each of the binary features contains the independent information about whether this type of disease is normal or abnormal. Then, it is available to conduct the counterfactual sample synthesis on these disease binary features.

Counterfactual Sample Synthesis. After obtaining the binary features $F = \{f_i\}_{i=1}^{N_c}$, where N_c stands for the number of disease categories in the datasets and d is the dimensions of the features, we start to synthesize counterfactual samples. The overall and detailed procedures are separately shown in Fig. 3 and Alg. 1. Specifically, given a original data (F, Y) that contains binary features F and the corresponding report Y , we first randomly pop one sentence s from Y , denoted as $s, Y^- \leftarrow Pop(Y)$ where Y^- is the

report without s . Then, the CheXbert [26] labeler¹ (LE) is adopted to identify the disease labels l described in the sentence s , denoted as $l \leftarrow LE(s)$. Then, we mask the corresponding binary features in F to get the counterfactual augmented binary features F^- as follows:

$$F^- = \{f_1, f_m, \dots, f_{N_c}\} \leftarrow \{f_i\}_{i=1}^{N_c} \quad (5)$$

where f_m denotes the masked binary features. It is worth noting that some certain type of diseases might be merged into one sentence when all of they are normal, thus we mask all the corresponding binary features in l . As a result, CSS produces the synthesized counterfactual samples (F^-, Y^-) where the corresponding disease features and their description sentence are masked, breaking the spurious coupling of the masked diseases to others, leading to the independence between diseases.

3.2.2 CRR

The sentence coherence coupling is also a spurious confounder as analysed above, which causes the conditional effect of diseases. To solve this problem, it is required to break the sentence coherence in the RRG reports. In this paper, we propose a simple-but-effective CRR strategy that randomly reconstructs the sentences in reports. Specifically, instead of treating a complete medical report as a whole label, we propose to regard each sentence as an independent component. Thus, it is realizable to conduct the counterfactual augmentation in the sentence level to break the coherence between sentences while maintain the information of each sentences. Under this kind of ideology, for the given report Y , we randomly reconstruct $re-con(\cdot)$ the orders of sentences as follows:

$$Y^+ \leftarrow re-con(\{s_i\}_{i=1}^{N_T}) \quad (6)$$

where Y^+ stands for the counterfactual augmented report breaking the spurious sentence coherence confounder while maintaining other critical causal information for RRG.

To further improve the accuracy though integrating the strengths of CSS and CRR, as illustrated in Alg. 1, we conduct the counterfactual augmentation with CSS and CRR serially. The original data is first processed by the CSS to break the spurious visual coupling and then processed by CRR for breaking the spurious sentence coherence coupling, resulting the ensemble counterfactual augmented data (F^-, Y^+) .

4. Experiments

4.1. Datasets and Evaluation Metrics

To evaluate the effectiveness of our proposed method, we adopt the widely-used IU X-Ray dataset [7] and MIMIC-

¹<https://github.com/stanfordmlgroup/CheXbert>

CXR dataset [11]. We evaluate our proposed approach on the widely used Neural Language Generation (NLG) metrics: BLEU-4 (B-4) [22], ROUGE-L (R-L) [16] and METEOR (M) [2]. Besides, Accuracy (A), Precision (P), Recall (R) and F1-score (F1) are taken as the indicator for Clinical Efficacy (CE) estimate. It is worth noting that we assume CE metrics are much more critical in the Radiology Report Generation (RRG) task, so we value more on them in this paper but regard NLG metrics as auxiliary metrics.

4.2. Implementation Details

We use the ResNet-101 [9] pretrained on ImageNet [8] as the backbone Binary Feature Extraction model to extract binary visual features of radiographs. The disease categories N_c is 14, and the dimension of each extracted visual feature map are set to 2048. In addition, following the previous works [6, 18], we use images as input for IU X-Ray dataset, which contains the frontal and lateral views, and use single image as input for MIMIC-CXR dataset. We concatenate the feature maps of the frontal and lateral view of images together for IU X-Ray dataset. Moreover, models are trained for 40 and 20 epochs respectively on IU X-Ray and MIMIC-CXR datasets using cross-entropy loss and adopt ADAM optimizer [13]. We set the initial learning rate to 1e-4 and delay by 0.9 per epoch. The beam size is set to 3.

4.3. Results and Analyses

We propose a model-free general counterfactual data augmentation method, which means it could be applied in any models to improve the accuracy of RRG task. And we conduct experiments on several common open-source baseline models of RRG task, i.e., Vanilla Transformer [29] and R2Gen [6]. We first explore effects of our two sub-methods, i.e., the Counterfactual Sample Synthesis (CRR) and the Counterfactual Report Reconstruction (CRR), and the effects of augmentation rates with the ablation studies on baseline models on CE metrics. Additionally, we conduct the experiments about the overall CE and NLG performance comparison with state-of-the-art (SOTA) RRG methods as well as the accuracy of each type of diseases. Finally, the visualization of the generated report comparison are shown to demonstrate the effects of our method.

4.3.1 Ablation Studies

We conduct the ablation studies on IU X-Ray datasets to evaluate the effectiveness of our proposed sub-methods, i.e., the CSS and the CRR, as well as their ensemble ability, where the results are shown in Tab. 2.

Effects of Counterfactual Sample Synthesis. We propose a novel CSS method to breaking the one-to-many spurious joint visual coupling between visual features to the disease labels. From the results of baseline models and their

Table 2. Ablation studies of our proposed sub-methods CSS and CRR, and their ensemble on the baseline models.

Datasets	Methods	A	P	R	F1
IU X-Ray	Vanilla	0.914	0.398	0.404	0.411
	/w CSS	0.928	0.493	0.506	0.500
	/w CRR	0.927	0.441	0.502	0.469
	/w CSS & CRR	0.928	0.497	0.511	0.504
	R2Gen	0.914	0.411	0.414	0.412
	/w CSS	0.930	0.512	0.524	0.518
	/w CRR	0.922	0.455	0.468	0.462
	/w CSS & CRR	0.931	0.517	0.531	0.523
MIMIC-CXR	Vanilla	0.782	0.256	0.427	0.320
	/w CSS	0.793	0.285	0.472	0.355
	/w CRR	0.782	0.270	0.432	0.332
	/w CSS & CRR	0.801	0.348	0.507	0.413
	R2Gen	0.786	0.287	0.446	0.350
	/w CSS	0.800	0.348	0.503	0.411
	/w CRR	0.794	0.317	0.478	0.381
	/w CSS & CRR	0.805	0.358	0.519	0.424

cooperation with *w CR* in the Tab. 2, every baseline models show an exciting increasing trends when they are applied with our CSS method. This remarkable performance improvement might give the credit to the decoupling ability of our CSS method which breaks the spurious coupling between visual features through randomly masking the visual features and their corresponding describing sentences. This counterfactual augmentation operation has the ability to improve the independence between visual features which force models to learn to determine the results conditioned on the truth visual features.

Effects of Counterfactual Report Reconstruction.

The CRR method is proposed to break the spurious coherence of radiology sentence that leads to the conditional sentence coherence coupling, for which the counterfactual augmentation operation is solely conducted on the reports of RRG task. From the results of baseline models and their cooperation with *w CRR* in Tab. 2, there is also an astonishing growth when the baseline models applied with our CRR method. We assume that the counterfactual augmentation operation which randomly reconstructs the sequence orders of sentences in report breaking the spurious conditional sentence coherence coupling. Additionally, based on our temporal causal graph, when applied with our CRR method, the generation of each token will only rely on the visual features and the previous generated tokens inside the sentence, rather than being influenced by the tokens generated in the previous sentences or rather the co-occurrences of diseases.

Ensemble. The *w CSS & CRR* indicates the effectiveness of the ensemble of our two sub-methods, where the results of baseline models equipped with the ensemble methods show an increment than all the ablation models with

Table 3. Ablation studies of our counterfactual augmentation rates based on baseline Vanilla model on MIMIC-CXR datasets.

Rates	A	P	R	F1
-	0.782	0.256	0.427	0.320
25%	0.801	0.300	0.506	0.377
50%	0.803	0.337	0.504	0.404
75%	0.800	0.345	0.504	0.409
100%	0.801	0.348	0.507	0.413

sole sub-method. This improvement demonstrates that our two proposed counterfactual augmentation sub-methods are model-free general methods which could be easily applied on all the RRG models to improve the accuracy of the generated reports. Besides, the two sub-methods will not mutually interfere where the abilities shown in Tab. 2 are even better when models equipped them together.

Counterfactual Augmentation Rates. Tab. 3 shows the results of the baseline Vanilla model applied with different rates of our counterfactual augmentation method. It could be easily concluded that the CE metrics of generated reports shows an overall increasing tends when conducting higher rate of our method. This phenomenon in the ablation results indicates that our hypothesis that the disease co-occurrence is a spurious confounder. Additionally, with more spurious data being interfered, the RRG models are guided to learn the causal information that produce more accurate reports, which introduces a novel and reliable research interest and boosts the progress in RRG field.

Table 4. Comparison of the proposed strategy applied on the widely compared baselines with the SOTA RRG models on MIMIC-CXR datasets. The higher score indicates better performance, and we denote the best score to bold. The † means the models are implemented by ourselves.

Methods	Year	NLG Metrics			CE Metrics		
		B-4	M	R-L	P	R	F1
CMN [5]	2021	0.106	0.142	0.278	0.334	0.275	0.278
CA [19]	2021	0.109	0.151	0.283	0.352	0.298	0.303
MSA [33]	2022	0.118	-	0.287	-	-	-
CMM&RL [25]	2022	0.109	0.151	0.287	0.342	0.294	0.292
CMCA [27]	2022	0.117	0.148	0.287	0.444	0.297	0.356
Cvt-21 [21]	2023	0.124	0.153	0.285	0.359	0.412	0.384
M2KT [34]	2023	0.111	-	0.274	0.420	0.339	0.352
ORGAN [10]	2023	0.123	0.162	0.293	0.416	0.418	0.385
DCL [15]	2023	0.109	0.150	0.284	0.471	0.352	0.373
Vanilla † [29]	2017	0.100	0.129	0.274	0.256	0.427	0.320
/w Ours †	-	0.056	0.105	0.230	0.348	0.507	0.413
R2Gen † [6]	2020	0.092	0.130	0.265	0.287	0.446	0.350
/w Ours †	-	0.058	0.106	0.229	0.358	0.519	0.424

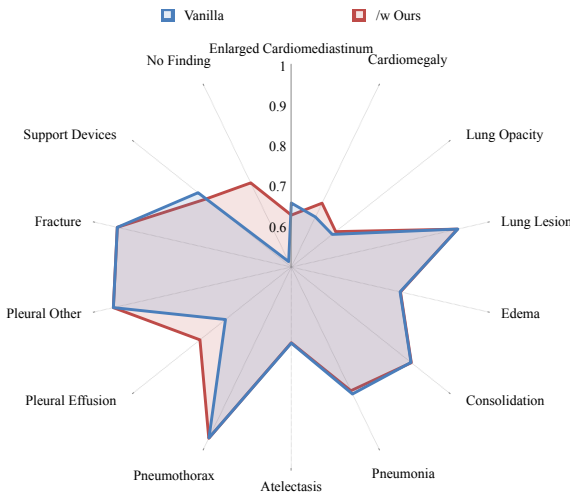


Figure 4. Comparison of abnormality classification results (Accuracy) of 14 diseases on MIMIC-CXR datasets.

4.3.2 Comparison with SOTA

Tab. 4 shows the comparison of our proposed counterfactual augmentation strategy applied on baselines with the SOTA RRG models. It is worth noting that our model-free general strategy could be applied on all of these SOTA models, but we only evaluate our strategy on the widely compared models with public codes. We directly quote most results from the original papers for the comparison methods, while implement the baseline models by ourselves denoted as †. Besides, we only conduct comparisons on MIMIC-CXR datasets because most of the SOTA models only provided their NLG metrics on IU X-Ray datasets in their works

while the CE metrics are blank.

Some results and analyses could be concluded based on Tab. 4 and Fig. 4. First, there is a remarkable increasing on all the CE metrics when the baseline models applied with our counterfactual augmentation strategy, which indicates that our strategy is capable of increasing the accuracy of the generated reports. Additionally, some CE metrics are even better than the SOTA models especially on the Recall and F1-score. These improvements are exciting because they indicate that our strategy employed by the most basic RRG models could result in a commensurate or even superior performance on the accuracy of the generated reports.

However, there is a decline on NLG metrics when the baseline models applying our counterfactual augmentation strategy. We assume that this decline is caused by our CRR method which break the coherence between sentences. As our rethinking, the sentences in reports are independent because each sentence describes certain types of diseases independently, which means the orders of sentence sequences are meaningless. However, the NLG metrics used in RRG task are inherited from the traditional Machine Translation and Image Captioning tasks, both of which regard the generated results as an integrated whole where each sentence is coherent with the context. In this case, the junctions between sentences are also considered as effective gram hits, such as grams containing '.', which confuses the performance of the generated reports, increases the NLG results of SOTA models, but decreases ours. Besides, the decline of precision might because the report labelers are different where our method and ORGAN [10] adopt the Chexbert labeler to label our generated report while others used Chexpert labeler.

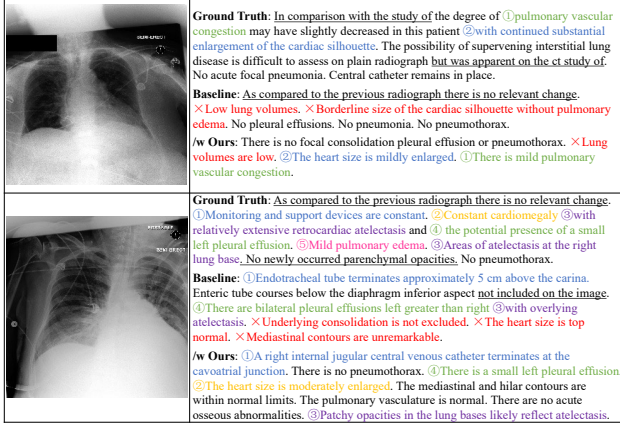


Figure 5. Visualization of the comparison of ground truth reports, the reports generated by the baseline Vanilla model and Vanilla with our method on MIMIC-CXR datasets. The serial numbers with various colors are sentences describing the abnormal findings. Red colored sentences with 'x' denote the sentences are wrong to the radiographs. The underlined sentences contain information that does not present in the radiographs.

4.3.3 Visualization

We also visualize the report generated by the baseline Vanilla model and its combinations with our method, where the results are shown in Fig. 5. First, from the comparison of colored sentences with serial numbers, it is obvious that models applied our method could effectively identify more disease information and generate more accurate reports. Additionally, compared the red colored sentences with 'x', the baseline models generate more sentences that are not correctly reflecting to the information in radiographs. Besides, the underlined sentences contains information that not appeared in the radiographs, which means that the ground truth reports includes some amounts of spurious and confusing information that could not be found in the corresponding radiographs, which will hurt the model performances. For example, as shown in Fig. 5 the baseline models also generate those meaningless sentences. Fortunately, models applied with our method show much less underlined sentences. We assume that this performance improvement could give the credit to that our method help the models to focus on the critical visual features and reduce the dependence between sentences, instead of generating report relying on the co-occurrence of diseases.

5. Conclusion

From a new perspective of statistics and causality, we rethink and reason the causes and effects of the spurious disease co-occurrence on RRG tasks. Specifically, based on the Simpson’s paradox, we discuss the causes of disease co-occurrence in RRG tasks and point out that it is a spurious

confounder that leads to two aspects of couplings, i.e., the Joint Vision Coupling C_j and Conditional Sentence Coherence Coupling C_c . Then, the causal graph is used to clarify the impact mechanism of C_j and C_c on RRG. Based on the rethinking, an easy-but-effective general counterfactual augmentation method is proposed, which contains the two sub-methods, i.e., the Counterfactual Sample Synthesis and the Counterfactual Report Reconstruction, to solve the two problems caused by the two spurious confounders respectively. Experiments conducted on two widely used datasets and further result analyses demonstrate the value of our re-thinking on RRG task and the ability of our proposed methods to solve these problems.

Limitations. While we emphasize the accuracy in medicine scenes, reports generated using our counterfactual augmentation strategy show a decline on Natural Language Generation (NLG) metrics. However, these NLG metrics designed to evaluate the consistency of a whole paragraph might not be suitable for RRG task because of the independence between sentences. To solve this limitation, we will research to propose an appropriate NLG metric for RRG task in future works.

References

- [1] Tadas Baltrušaitis, Chaitanya Ahuja, and Louis-Philippe Morency. Multimodal machine learning: A survey and taxonomy. *IEEE T. Pattern Anal.*, 41(2):423–443, 2018. [1](#), [3](#)
- [2] Satanjeev Banerjee and Alon Lavie. Meteor: An automatic metric for mt evaluation with improved correlation with human judgments. In *ACL Workshop*, pages 65–72, 2005. [6](#)
- [3] Peter J Bickel, Eugene A Hammel, and J William O’Connell. Sex bias in graduate admissions: Data from berkeley: Measuring bias is harder than is usually assumed, and the evidence is sometimes contrary to expectation. *Science*, 187(4175):398–404, 1975. [3](#)
- [4] Long Chen, Yuhang Zheng, Yulei Niu, Hanwang Zhang, and Jun Xiao. Counterfactual samples synthesizing and training for robust visual question answering. *IEEE T. Pattern Anal.*, 45(11):13218–13234, 2023. [5](#)
- [5] Zhihong Chen, Yaling Shen, Yan Song, and Xiang Wan. Cross-modal memory networks for radiology report generation. In *ACL-IJCNLP*, pages 5904–5914, 2021. [8](#)
- [6] Zhihong Chen, Yan Song, Tsung-Hui Chang, and Xiang Wan. Generating radiology reports via memory-driven transformer. In *EMNLP*, pages 1439–1449, 2020. [4](#), [6](#), [8](#)
- [7] Dina Demner-Fushman, Marc D Kohli, Marc B Rosenman, Sonya E Shooshan, Laritza Rodriguez, Sameer Antani, George R Thoma, and Clement J McDonald. Preparing a collection of radiology examinations for distribution and retrieval. *J. Am. Med. Inform. Assn.*, 23(2):304–310, 2016. [2](#), [6](#)
- [8] Jia Deng, Wei Dong, Richard Socher, Li-Jia Li, Kai Li, and Li Fei-Fei. Imagenet: A large-scale hierarchical image database. In *CVPR*, pages 248–255, 2009. [6](#)

[9] Kaiming He, Xiangyu Zhang, Shaoqing Ren, and Jian Sun. Deep residual learning for image recognition. In *CVPR*, pages 770–778, 2016. 6

[10] Wenjun Hou, Kaishuai Xu, Yi Cheng, Wenjie Li, and Jiang Liu. Organ: Observation-guided radiology report generation via tree reasoning. In *ACL*, pages 8108–8122, 2023. 1, 4, 8

[11] Alistair EW Johnson, Tom J Pollard, Nathaniel R Greenbaum, Matthew P Lungren, Chih-ying Deng, Yifan Peng, Zhiyong Lu, Roger G Mark, Seth J Berkowitz, and Steven Horng. Mimic-cxr-jpg, a large publicly available database of labeled chest radiographs. *arXiv*, 2019. 2, 6

[12] Andrej Karpathy and Li Fei-Fei. Deep visual-semantic alignments for generating image descriptions. In *CVPR*, pages 3128–3137, 2015. 1

[13] Diederik P Kingma and Jimmy Ba. Adam: A method for stochastic optimization. *arXiv*, 2014. 6

[14] Christy Y Li, Xiaodan Liang, Zhiting Hu, and Eric P Xing. Knowledge-driven encode, retrieve, paraphrase for medical image report generation. In *AAAI*, volume 33, pages 6666–6673, 2019. 1

[15] Mingjie Li, Bingqian Lin, Zicong Chen, Haokun Lin, Xiaodan Liang, and Xiaojun Chang. Dynamic graph enhanced contrastive learning for chest x-ray report generation. In *CVPR*, pages 3334–3343, 2023. 3, 8

[16] Chin-Yew Lin. Rouge: A package for automatic evaluation of summaries. In *Text Summarization Branches Out*, pages 74–81, 2004. 6

[17] Fenglin Liu, Shen Ge, and Xian Wu. Competence-based multimodal curriculum learning for medical report generation. In *ACL-IJCNLP*, pages 3001–3012, 2021. 3

[18] Fenglin Liu, Xian Wu, Shen Ge, Wei Fan, and Yuexian Zou. Exploring and distilling posterior and prior knowledge for radiology report generation. In *CVPR*, pages 13753–13762, 2021. 1, 2, 3, 4, 6

[19] Fenglin Liu, Changchang Yin, Xian Wu, Shen Ge, Ping Zhang, and Xu Sun. Contrastive attention for automatic chest x-ray report generation. In *IJCNLP*, pages 269–280, 2021. 8

[20] Qi Liu, Matt Kusner, and Phil Blunsom. Counterfactual data augmentation for neural machine translation. In *NAACL*, pages 187–197, 2021. 5

[21] Aaron Nicolson, Jason Dowling, and Bevan Koopman. Improving chest x-ray report generation by leveraging warm starting. *Artif. Intell. Med.*, 144:102633, 2023. 8

[22] Kishore Papineni, Salim Roukos, Todd Ward, and Wei-Jing Zhu. Bleu: a method for automatic evaluation of machine translation. In *ACL*, pages 311–318, 2002. 6

[23] Judea Pearl, Madelyn Glymour, and Nicholas P Jewell. *Causal inference in statistics: A primer*. John Wiley & Sons, 2016. 2

[24] Silviu Pitis, Elliot Creager, and Animesh Garg. Counterfactual data augmentation using locally factored dynamics. In *NeurIPS*, volume 33, pages 3976–3990, 2020. 5

[25] Han Qin and Yan Song. Reinforced cross-modal alignment for radiology report generation. In *ACL*, pages 448–458, 2022. 8

[26] Akshay Smit, Saahil Jain, Pranav Rajpurkar, Anuj Pareek, Andrew Y Ng, and Matthew Lungren. Combining automatic labelers and expert annotations for accurate radiology report labeling using bert. In *EMNLP*, pages 1500–1519, 2020. 6

[27] Xiao Song, Xiaodan Zhang, Junzhong Ji, Ying Liu, and Pengxu Wei. Cross-modal contrastive attention model for medical report generation. In *COLING*, pages 2388–2397, 2022. 3, 4, 8

[28] Tim Tanida, Philip Müller, Georgios Kaassis, and Daniel Rueckert. Interactive and explainable region-guided radiology report generation. In *CVPR*, pages 7433–7442, 2023. 1, 2, 4

[29] Ashish Vaswani, Noam Shazeer, Niki Parmar, Jakob Uszkoreit, Llion Jones, Aidan N Gomez, Łukasz Kaiser, and Illia Polosukhin. Attention is all you need. In *NeurIPS*, volume 30, 2017. 6, 8

[30] Oriol Vinyals, Alexander Toshev, Samy Bengio, and Dumitru Erhan. Show and tell: A neural image caption generator. In *CVPR*, pages 3156–3164, 2015. 1

[31] Fuyu Wang, Xiaodan Liang, Lin Xu, and Liang Lin. Unifying relational sentence generation and retrieval for medical image report composition. *IEEE T. Cybernetics*, 52(6):5015–5025, 2022. 1, 2

[32] Jingwei Wang, Jianshan He, Weidi Xu, Ruopeng Li, and Wei Chu. Learning to discover various simpson’s paradoxes. In *ACM KDD*, pages 5092–5103, 2023. 3

[33] Zhanyu Wang, Hongwei Han, Lei Wang, Xiu Li, and Luping Zhou. Automated radiographic report generation purely on transformer: A multicriteria supervised approach. *IEEE T. Med. Imaging*, 41(10):2803–2813, 2022. 8

[34] Shuxin Yang, Xian Wu, Shen Ge, Zhuozhao Zheng, S Kevin Zhou, and Li Xiao. Radiology report generation with a learned knowledge base and multi-modal alignment. *Med. Image Anal.*, 86:102798, 2023. 8

[35] Junsan Zhang, Xiuxuan Shen, Shaohua Wan, Sotirios K. Goudos, Jie Wu, Ming Cheng, and Weishan Zhang. A novel deep learning model for medical report generation by inter-intra information calibration. *IEEE J. Biomed. Health*, 27(10):5110–5121, 2023. 1

[36] Yixiao Zhang, Xiaosong Wang, Ziyue Xu, Qihang Yu, Alan Yuille, and Daguang Xu. When radiology report generation meets knowledge graph. In *AAAI*, volume 34, pages 12910–12917, 2020. 1, 2, 3

[37] Yongsen Zheng, Jinghui Qin, Pengxu Wei, Ziliang Chen, and Liang Lin. Cipl: Counterfactual interactive policy learning to eliminate popularity bias for online recommendation. *IEEE T. Neur. Net. Lear.*, pages 1–14, 2023. 4